

A Behavior-Based Visual Servoing Control Law

Mohammed Marey¹ & François Chaumette

IRISA/INRIA-Rennes, Campus de Beaulieu, 35042 Rennes, France.
(e-mail: Firstname.Name@irisa.fr)

Abstract: In this paper, we analyze and compare four image-based visual servoing control laws. Three of them are classical while a new one is proposed. This new control law is based on a behavior controller to adjust the movement of the camera. It can also be used to switch between the classical methods. An analytical study of all control schemes when translational motion along and rotational motion around the optical axis is also presented. Finally, simulation and experimental results show that the new control law with a behavior controller has a wider range of success than the other control schemes and can be used to avoid local minima and singularities.

Keywords: visual servoing, robotics control, singularities, local minima.

1. INTRODUCTION

Visual servoing is a well known approach to increase the accuracy, the versatility and the robustness of a vision-based robotic system [11, 5]. Two main aspects have a great impact on the behavior of any visual servoing scheme: the selection of the visual features used as input of the control law and the form of the control scheme. As for the visual features, they can be selected in the image space (point coordinates, parameters representing straight lines or ellipses, moments,... [8, 12, 6, 9, 4]), in the Cartesian space (pose, coordinates of 3D points,... [16, 18]), or composed of a mixture of both kinds of features attempting to incorporate the advantages of both image-based and position-based methods [13, 7, 2]. As for the choice of the control law [8, 14, 5], it affects the behavior of the selected visual features (local or global exponential decrease, second order minimization, ...) and may lead, or not, to local minima and singularities [3].

This paper is not concerned with the choice of the visual features, but with the analysis of different control schemes. That is why we will consider the most usual and simple features, that are the Cartesian coordinates of image points. As for the control schemes, we consider three classical control laws and we also propose in this paper a new control law that follows an hybrid strategy. It is based on a behavior parameter that can be used to tune the weight of the current and the desired interaction matrix in the control law. We will see that in some configurations where all other control schemes fail, this new control law allows the system to converge. The paper also includes an analysis of the control laws with respect to translational motion along and rotational motion around the optical axis. As we will see, a singularity of the control law proposed in [14] will be exhibited thanks to this analysis.

The paper is organized as follows: In Section 2, classical control schemes are recalled from which the control law with a behavior controller is proposed. In Section 3, an analysis of the control laws in the presence of rotation and translation w.r.t. the camera optical axis is presented. Finally, experimental and simulation results are presented in Section 4.

2. NEW CONTROLLER WITH A BEHAVIOR PARAMETER

Let $\mathbf{s} \in \mathbb{R}^k$ be the vector of the selected k visual features, \mathbf{s}^* their desired value and $\mathbf{v} \in \mathbb{R}^6$ the instantaneous velocity of the camera. Most classical control laws have the following form:

$$\mathbf{v} = -\lambda \widehat{\mathbf{L}}_{\mathbf{s}}^+ (\mathbf{s} - \mathbf{s}^*) \quad (1)$$

where λ is a gain and $\widehat{\mathbf{L}}_{\mathbf{s}}^+$ is the pseudoinverse of an estimation or an approximation of the interaction matrix related to \mathbf{s} (defined such that $\dot{\mathbf{s}} = \mathbf{L}_{\mathbf{s}} \mathbf{v}$ where $\mathbf{v} = (v, \omega)$ with v the translational velocity and ω the rotational one). Different forms for $\widehat{\mathbf{L}}_{\mathbf{s}}$ have been proposed in the past [8, 14, 5]. For simplicity, we consider that all values can be computed accurately, leading to the following choices

$$1) : \widehat{\mathbf{L}}_{\mathbf{s}} = \mathbf{L}_{\mathbf{s}^*} \quad (2)$$

$$2) : \widehat{\mathbf{L}}_{\mathbf{s}} = \mathbf{L}_{\mathbf{s}(t)} \quad (3)$$

$$3) : \widehat{\mathbf{L}}_{\mathbf{s}} = (\mathbf{L}_{\mathbf{s}^*} + \mathbf{L}_{\mathbf{s}(t)})/2. \quad (4)$$

In the first case, $\widehat{\mathbf{L}}_{\mathbf{s}}$ is constant during all the servo since it is the value of the interaction matrix computed at the desired configuration. In the second case, $\widehat{\mathbf{L}}_{\mathbf{s}}$ changes at each iteration of the servo since the current value of the interaction matrix is used. Finally, in the third case, the average of these two values is used [14]. These three usual choices for $\widehat{\mathbf{L}}_{\mathbf{s}}$ when used with (1) define three distinct control laws, that we will denote D, C and A (for desired, current and average respectively) in the remainder of the paper.

As explained in [17], it is possible to improve the behavior of control law A by using:

$$\widehat{\mathbf{L}}_{\mathbf{s}} = (\mathbf{L}_{\mathbf{s}^*} {}^{c^*}\mathbf{T}_{\mathbf{c}} + \mathbf{L}_{\mathbf{s}(t)})/2$$

where ${}^{c^*}\mathbf{T}_{\mathbf{c}}$ is the spatial motion transform matrix to transform velocities expressed in the desired camera frame to the current camera frame. However, we will not consider this supplementary control scheme in the following.

On one hand, near the desired pose where the error $\mathbf{s} - \mathbf{s}^*$ is low, the same behavior is obtained whatever the choice of $\widehat{\mathbf{L}}_{\mathbf{s}}$

¹ Mohammed Marey is granted by the Egyptian Government.

since we have in that case $\mathbf{L}_{s(t)} \approx \mathbf{L}_{s^*}$. On the other hand, as soon as $\mathbf{s} - \mathbf{s}^*$ is large, it is well known that the choice of $\widehat{\mathbf{L}}_s$ induces a particular behavior of the system since we thus have $\mathbf{L}_{s(t)} \neq \mathbf{L}_{s^*}$. This motivates the current research on the determination of visual features such that the interaction matrix is constant in all the configuration space of the camera, but it is clearly still an open problem, and, as already said, not the subject of this paper.

From (2), (3) and (4), a general form for $\widehat{\mathbf{L}}_s$ can easily be written by introducing a behavior controller $\beta \in \mathbb{R}$

$$\widehat{\mathbf{L}}_s = \mathbf{L}_\beta = (\beta \mathbf{L}_{s^*} + (1 - \beta) \mathbf{L}_{s(t)}). \quad (5)$$

Using (5) in (1), we obtain a new control law, denoted G in the following (for “general”). Control laws D, C, and A are known to be locally asymptotically stable only [5]. The same is also true for control law G. Of course, if $\beta = 1$, we find again control law D, if $\beta = 0$, we obtain control law C, and if $\beta = 1/2$ we obtain control law A. Control law G could thus be used to switch between the different control schemes during the execution of the task. Switching strategies have already been proposed in [10, 1] but, in these works, switching is performed between image-based and position-based approaches, that is between different features, while here the features are the same but their control would be different.

In this paper, we are not interested in designing a possible strategy to switch between the different control laws. We are looking if particular values of β provide a better behavior of the system. Indeed, the main interesting property of control law G obtained using (5) is that the behavior of the system changes gradually from the behavior using control law C to the behavior using control law A when β varies from 0 to 1/2, and similarly, the behavior changes gradually from the behavior using control law A to the behavior using control law D when β varies from 1/2 to 1. Hence, this new control scheme allows us to adapt the behavior of the system based on the selected value of β . We will see in Section 4.1 that particular values of β indeed allows the system to converge while the other control schemes fail for some configurations.

Let us finally note that in case of modeling or calibration errors, the matrices \mathbf{L}_{s^*} and $\mathbf{L}_{s(t)}$ have to be respectively replaced by approximations $\widehat{\mathbf{L}}_{s^*}$ and $\widehat{\mathbf{L}}_{s(t)}$, but that does not change the general properties of the control schemes as long as the approximations are not too coarse.

3. MOTION ALONG AND AROUND THE OPTICAL AXIS

This section presents an analytical analysis of the control laws described previously when the camera displacement is a combination of a translation t_z and a rotation r_z w.r.t. the camera optical axis. As usually done in IBVS, we have considered an object composed of four points forming a square.

The study includes two cases in which the movement along z -axis is from Z to Z^* and where $r_z = 90^\circ$ in the first case and $r_z = 180^\circ$ in the second case. In both cases, the object plane is parallel to the image plane.

The coordinates of a 3D point in the camera frame are denoted (X, Y, Z) and the coordinates of that point on the image plane are given by $\mathbf{x} = (x, y)$ with $x = X/Z$ and $y = Y/Z$. It is well known that the interaction matrix related to \mathbf{x} is given by

$$\mathbf{L}_x = \begin{bmatrix} -\frac{1}{Z} & 0 & \frac{x}{Z} & xy & -(1+x^2) & y \\ 0 & -\frac{1}{Z} & \frac{y}{Z} & 1+y^2 & -xy & -x \end{bmatrix}$$

Using four points, the visual feature vector \mathbf{s} is $\mathbf{s} = (x_0, x_1, x_2, x_3, y_0, y_1, y_2, y_3)$ whose desired value is $\mathbf{s}^* = (x_0^*, x_1^*, x_2^*, x_3^*, y_0^*, y_1^*, y_2^*, y_3^*)$.

Case 1: $r_z = 90^\circ$ & $t_z = (Z \rightarrow Z^)$* The coordinates of the four points w.r.t. the camera frame at the initial and the desired poses are denoted $p_{i0} = (-L, -L, Z)$, $p_{i1} = (-L, L, Z)$, $p_{i2} = (L, L, Z)$, $p_{i3} = (L, -L, Z)$, $p_{d0} = (-L, L, Z^*)$, $p_{d1} = (L, L, Z^*)$, $p_{d2} = (L, -L, Z^*)$ and $p_{d3} = (-L, -L, Z^*)$. Let $l = L/Z$ and $l^* = L/Z^*$. The initial value of \mathbf{s} is then $\mathbf{s}_i = (-l, -l, l, l, -l, l, l, -l)$, the desired value is $\mathbf{s}^* = (-l^*, l^*, l^*, -l^*, l^*, l^*, -l^*, -l^*)$ and $\mathbf{s}_i - \mathbf{s}^* = (-l + l^*, -l - l^*, l^* - l, l + l^*, -l - l^*, l - l^*, l + l^*, l^* - l)$ is the error vector. Using the analytical form of \mathbf{L}_x , it is possible to compute the analytical form of \mathbf{L}_β defined in (5) and then its pseudoinverse \mathbf{L}_β^+ . Using $Z = l^* Z^* / l$, we obtain after computations and simplifications

$$\mathbf{L}_\beta^+ = \begin{bmatrix} -c_0 & -c_0 & -c_0 & -c_0 & -c_1 & c_1 & -c_1 & c_1 \\ -c_1 & c_1 & -c_1 & c_1 & -c_0 & -c_0 & -c_0 & -c_0 \\ -c_3 & c_4 & c_3 & -c_4 & c_4 & c_3 & -c_4 & -c_3 \\ -c_5 & c_5 & -c_5 & c_5 & 0 & 0 & 0 & 0 \\ 0 & 0 & 0 & 0 & c_5 & -c_5 & c_5 & -c_5 \\ c_7 & c_6 & -c_6 & -c_7 & c_6 & -c_7 & -c_6 & c_7 \end{bmatrix}$$

where, when $\beta \in [0; 1]$,

$$\begin{aligned} c_0 &= \frac{l^* Z^*}{4(\beta l^* + (1 - \beta)l)} \\ c_1 &= \begin{cases} 0 & \text{if } \beta l^{*2} = (1 - \beta)l^2 \\ c_0 \frac{\beta(1 + l^{*2}) + (1 - \beta)(1 + l^2)}{(\beta l^{*2} - (1 - \beta)l^2)} & \text{else.} \end{cases} \\ c_3 &= \frac{l^* Z^* (\beta l^* + (1 - \beta)l)}{8((1 - \beta)^2 l^3 + \beta^2 l^{*3})}, \quad c_4 = \frac{l^* Z^* (\beta l^* - (1 - \beta)l)}{8((1 - \beta)^2 l^3 + \beta^2 l^{*3})} \\ c_5 &= \begin{cases} 0 & \text{if } \beta l^{*2} = (1 - \beta)l^2 \\ \frac{-1}{4(\beta l^{*2} - (1 - \beta)l^2)} & \text{else.} \end{cases} \\ c_6 &= \frac{\beta l^{*2} + (1 - \beta)l^2}{8((1 - \beta)^2 l^3 + \beta^2 l^{*3})}, \quad c_7 = \frac{\beta l^{*2} - (1 - \beta)l^2}{8((1 - \beta)^2 l^3 + \beta^2 l^{*3})} \end{aligned}$$

Using the value of $\mathbf{s}_i - \mathbf{s}^*$, the initial velocity \mathbf{v}_i is easily deduced from (1) as

$$\mathbf{v}_i = (0, 0, v_z, 0, 0, \omega_z) \quad (6)$$

where

$$v_z = \frac{\lambda Z^* l^* (\beta l^{*2} - (1 - \beta)l^2)}{\beta^2 l^{*3} + (1 - \beta)^2 l^3}, \quad \omega_z = \frac{\lambda l^* (\beta l^* + (1 - \beta)l)}{\beta^2 l^{*3} + (1 - \beta)^2 l^3}$$

As expected, the initial camera motion consists in performing a translation combined with a rotation whose value only depends on image data and on the chosen value for β and λ . We can note that \mathbf{L}_β is singular if $\beta l^{*2} = (1 - \beta)l^2$. For instance, such a singularity occurs when $l = l^*$ (i.e. $Z = Z^*$) and $\beta = 1/2$, which is very surprising. The control law A proposed in [14] is thus singular for a pure rotation of 90° , which had not been exhibited before as far as we know. In fact, the only way to avoid this singularity whatever the value of l and l^* is to select $\beta = 0$ or $\beta = 1$. As can be seen on (6), this singularity has no effect on the computed velocity in perfect conditions, but, as we will see in Section 4.1, a quite unstable behavior is obtained in the presence of image noise or for configurations near that

singularity (such that for instance the object plane is almost parallel to the image plane).

When $Z = Z^*$ then $l = l^*$ and the initial velocity \mathbf{v}_i becomes

$$\mathbf{v}_i = \left(0, 0, \frac{\lambda Z^*(2\beta - 1)}{2\beta^2 - 2\beta + 1}, 0, 0, \frac{\lambda}{2\beta^2 - 2\beta + 1} \right).$$

In that classical case, the velocity \mathbf{v}_i contains an unexpected translation whose direction depends on the value of β ($v_z < 0$ if $\beta < 1/2$ and $v_z > 0$ if $\beta > 1/2$). The only way to avoid this nonzero translation is to select $\beta = 1/2$ as already shown in [14], but \mathbf{L}_β is singular in that case...

Coming back to the more general case and setting $\beta = 1$ in \mathbf{L}_β^+ , the initial velocity \mathbf{v}_i using control law D is given by

$$\mathbf{v}_i = \left(0, 0, \lambda Z^*, 0, 0, \frac{\lambda l}{l^*} \right). \quad (7)$$

Whatever the value of Z , that is even when $Z < Z^*$ in which case the camera has to move backward, the initial camera motion contains a forward translational term. This surprising result extends the same property obtained when $Z = Z^*$ [5].

Setting $\beta = 0$, the initial velocity \mathbf{v}_i using the control law C is now

$$\mathbf{v}_i = \left(0, 0, \frac{-\lambda l^* Z^*}{l}, 0, 0, \frac{\lambda l}{l} \right). \quad (8)$$

In that case, the initial camera motion contains a backward translational term whatever the value of Z , that is even when $Z \geq Z^*$. We can even note that, more l is small, *i.e.* more Z is large, more the initial backward motion is large, which is even more surprising than the result obtained for $\beta = 1$. These results extend thus largely the property exhibited in [6] when $Z = Z^*$. By comparing (7) and (8), we can also note that the amplitude of the rotational motion using control laws D and C is surprisingly not the same as long as $l \neq l^*$, that is as soon as $Z \neq Z^*$.

Setting $\beta = 1/2$, the velocity \mathbf{v}_i using control law A is

$$\mathbf{v}_i = \left(0, 0, \frac{2\lambda Z^* l^* (l^{*2} - l^2)}{l^{*3} + l^3}, 0, 0, \frac{2\lambda l l^* (l + l^*)}{l^3 + l^{*3}} \right).$$

In that case, a good behavior is obtained since the translational motion is always in the expected direction ($v_z < 0$ when $l^* < l$, that is when $Z < Z^*$, $v_z > 0$ when $l^* > l$ ($Z > Z^*$), and, as already said, $v_z = 0$ when $l = l^*$ (where $Z = Z^*$ but where \mathbf{L}_β is singular).

Case 2: $r_z = 180^\circ$ & $t_z = (Z \rightarrow Z^)$* We now consider the more problematic case where the camera displacement is composed of a translation and of a rotation of 180° around the camera optical axis. In that case, $\mathbf{s}_i - \mathbf{s}^* = (l + l^*, -l - l^*, -l - l^*, l + l^*, -l - l^*, -l - l^*, l + l^*, l + l^*)$ and \mathbf{L}_β^+ is given by

$$\mathbf{L}_\beta^+ = \begin{bmatrix} -c_0 & -c_0 & -c_0 & -c_0 & -c_1 & c_1 & -c_1 & c_1 \\ -c_1 & c_1 & -c_1 & c_1 & -c_0 & -c_0 & -c_0 & -c_0 \\ -c_3 & c_3 & c_3 & -c_3 & c_3 & c_3 & -c_3 & -c_3 \\ -c_4 & c_4 & -c_4 & c_4 & 0 & 0 & 0 & 0 \\ 0 & 0 & 0 & 0 & c_4 & -c_4 & c_4 & -c_4 \\ c_5 & c_5 & -c_5 & -c_5 & c_5 & -c_5 & -c_5 & c_5 \end{bmatrix}$$

where, when $\beta \in [0; 1]$,



Fig. 1. Afma6 robot

$$\begin{aligned} c_0 &= \frac{l^* Z^*}{4(\beta l^{*2} + (1 - \beta)l)} \\ c_1 &= c_0 \frac{\beta(1 + l^{*2}) + (1 - \beta)(1 + l^2)}{\beta l^{*2} + (1 - \beta)l^2} \\ c_3 &= \begin{cases} 0 & \text{if } \beta l^{*2} = (1 - \beta)l^2 \\ \frac{l^* Z^*}{8(\beta l^{*2} - (1 - \beta)l^2)} & \text{else} \end{cases} \\ c_4 &= \frac{1}{4(\beta l^{*2} + (1 - \beta)l^2)} \\ c_5 &= \begin{cases} 0 & \text{if } \beta l^* = (1 - \beta)l \\ \frac{1}{8(\beta l^* - (1 - \beta)l)} & \text{else} \end{cases} \end{aligned}$$

Proceeding as before, we obtain using the value of $\mathbf{s}_i - \mathbf{s}^*$

$$\begin{aligned} \mathbf{v}_i &= (0, 0, v_z, 0, 0, 0) \\ \text{where } v_z &= \begin{cases} 0 & \text{if } \beta l^{*2} = (1 - \beta)l^2 \\ \frac{\lambda Z^* l^* (l + l^*)}{\beta l^{*2} - (1 - \beta)l^2} & \text{else.} \end{cases} \end{aligned}$$

In all cases, no rotational motion is produced while a translational motion is generally obtained, but when $\beta l^{*2} = (1 - \beta)l^2$ in which case \mathbf{L}_β is singular, leading to a repulsive local minimum where $v_z = 0$. Such a case occurs for instance when $Z = Z^*$ (*i.e.* $l = l^*$) and $\beta = 1/2$, which corresponds to the control law proposed in [14]. Another singularity occurs when $\beta l^* = (1 - \beta)l$, which is also the case when $l = l^*$ and $\beta = 1/2$.

Of course, when $Z = Z^*$, we find again the results given in [3]: a pure forward motion is involved when $\beta = 1$ and a pure backward motion is involved when $\beta = 0$. More generally, for $\beta = 1$ and $\beta = 0$, the direction of motion is the same (*i.e.* forward or backward) whatever the value of l and l^* , that is whatever the value of Z with respect to Z^* . For any other value of β , the direction of motion depends on the relative value of Z with respect to Z^* , but unfortunately, there does not exist any value of β that will give a good behavior in that case since no rotational motion is computed by the control law.

4. RESULTS

In this section, experimental and simulation results are given. They have been obtained using the ViSP library [15] in which the new control schemes have been implemented.

4.1 Experimental results : Singularities

The experimental results have been obtained on a six degrees of freedom robot as shown in Fig. 1. They allow to validate the analysis presented in the previous section about the motion along and around the optical axis. Note that the velocities are saturated to forbid the application of too high values which may be computed near a singularity. More precisely, all velocity

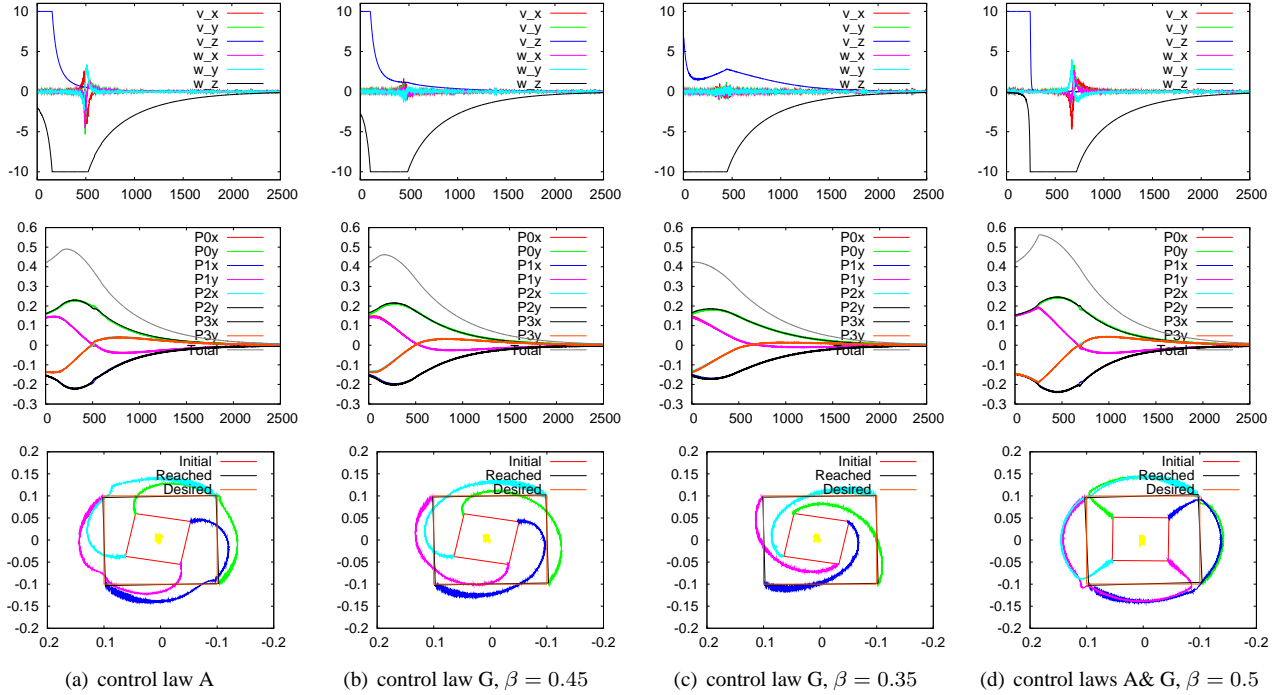


Fig. 2. Experimental results. Case A ($r_z = 170^\circ$ and $t_z = 0.5$ m) in (a), (b) and (c); case B ($r_z = 180^\circ$ and $t_z = 0.5$ m) in (d). Top line: camera velocity components (in m/s and rad/s), middle line: visual features error components and global error, bottom line: image points trajectories.

components are normalized when needed so that the maximal one is not more than 10 cm/s or 10 deg/s.

Case A In this first case, the required camera motion is composed of a rotation of 170° around the optical axis combined with a translation of 0.5 m along the optical axis toward the object (a square once again). As usual, gain λ has been set to 0.1. As expected unfortunately, control law D makes the points leave the camera field of view due to a forward motion, while control law C makes the robot reach its joints limits due to a backward motion. As can be seen in Fig. 2.a, control law A starts with high value of v_z toward the object, while ω_z increases until the translational motion is almost finished. As demonstrated in the analytical study, since the pure rotation $r_z = 90^\circ$ corresponds to a singularity of control law A, the behavior of the system is quite unstable near this configuration, that is from iterations 800 to 1200, as can be observed in Fig. 2.a. As can be seen in Fig. 2.b, using control law G with $\beta = 0.45$ enables to decrease significantly the effect of the singularity near $r_z = 90^\circ$, while its effect completely disappears for $\beta = 0.35$ (see Fig. 2.c).

Case B In this second case, the task is still to perform a translation of 0.5 m toward the object but combined now with a rotation of 180° . Figure 2.d shows the results obtained for control law A (that is G with $\beta = 0.5$). The velocity components show that the motion of the camera starts with a pure translation toward Z^* . From the analytical study, no rotational motion should occur. However, due to small image noise and to the use of a real robot, that is a non perfectly calibrated system, the robot moves away from the repulsive local minimum and starts to rotate. The effect of the singularity at 90° is clearly visible, but after its crossing, the system converges to the desired pose.

4.2 Simulation Results : Optical Axis Studies

A general description of the camera behavior when the required movement is along the optical axis with all possible values of r_z is now given. It has been obtained through extensive simulations. As for the experimental results, we have set $L = 0.1$, the initial camera pose is $(0, 0, 1, 0, 0, r_z)$, and the desired camera pose is $(0, 0, 0.5, 0, 0, 0)$ so that the square appears as a centered square in the image with $l^* = 0.2$ and $l = 0.1$. We have also set $\lambda = 0.1$ and saturation terms on the velocity components have been introduced.

Applying control law D, the camera rotates and translates toward the desired pose without any additional movement as soon as $r_z \leq 78^\circ$. When $r_z > 78^\circ$, the camera continues its translational motion after reaching $Z = Z^*$ and then moves back toward the desired pose. The translation increases as r_z increases (see Fig. 3.a). When $r_z \geq 155^\circ$, the control law fails since the camera reaches the object plane where $Z = 0$. Finally, v_z reaches its saturated maximal value at the first iteration of the control scheme while ω_z reaches its saturated value after several iterations (see Fig. 3.a).

Applying control law C, the camera rotates and translates correctly as long as $r_z \leq 61^\circ$. When $r_z > 61^\circ$, the camera starts moving backward and then translates forward. The backward translation increases as r_z increases (see Fig. 3.b). We can note on Fig. 3.b that the maximal rotational velocity is reached and saturated when the translational motion changes from backward to forward. The number of iterations required to reach the desired pose increases rapidly when $r_z > 150^\circ$. Finally, when $r_z \geq 178.6^\circ$, the backward translation is so large that the camera is not able to reach the desired pose.

Control law A converges with a perfect behavior (that is without any supplementary translation) as long as $r_z < 180^\circ$ (see

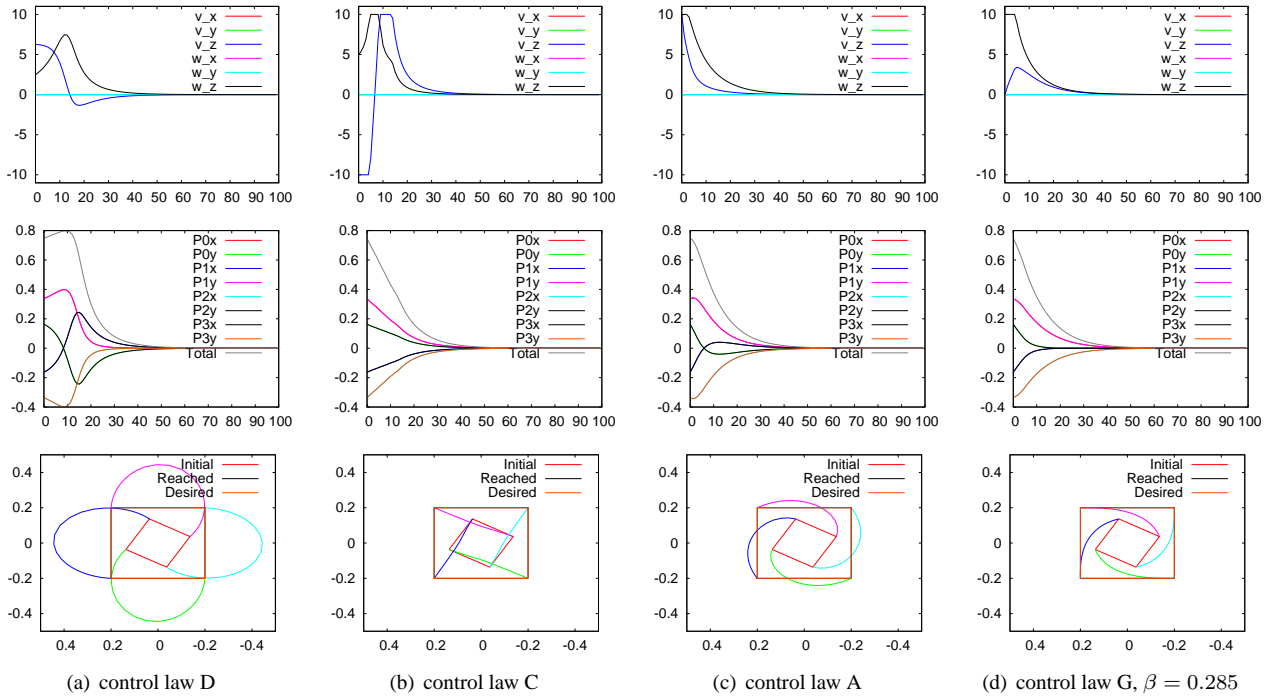


Fig. 3. Simulation results for optical axis studies obtained when $t_z = 0.5$ m and $r_z = 120^\circ$.

Fig. 3.c). As discussed before, control law A has a singularity when $r_z = 180^\circ$, that is why the velocity components are saturated at the beginning of the servo for large values of r_z .

Applying the new control law G, different behaviors are obtained based on the value selected for β . When the value of β is near to 0, 1 and 1/2, the behavior of the control law approaches the behavior of control laws C, D and A respectively. Best selection of β leads to enhance the behavior of the control law for a given displacement. For example, when $r_z = 120^\circ$, control law G allows the camera to reach its desired pose when $\beta \in [-0.08, 1.19]$ with the best behavior obtained when $\beta = 0.285$ (see Fig. 3.d). In that case, the rotational velocity ω_z reaches its maximum value at the first iteration. The error on each point coordinates starts also to decrease at the first iteration. When $r_z = 170^\circ$, the camera reaches its desired pose as long as $\beta \in [0.33, 0.85]$ with best behavior obtained when β is between 0.35 and 0.4.

4.3 Simulation results : Local Minima

Now, we consider a difficult configuration and compare the results obtained with the different control schemes described previously. A pose is denoted as $\mathbf{p} = (\mathbf{t}, \mathbf{r})$ where \mathbf{t} is the translation expressed in meter and \mathbf{r} the roll, pitch and yaw angles expressed in degrees. The desired camera pose is given by $(0, 0, 1, 45, -30, 30)$ which means that the desired position of the image plane is not parallel to the object. The initial camera pose is given by $(0, 0, 1, -46, 30, 30)$. As can be seen on Fig. 4.a, using control law D, the camera is first motionless, as in a local minimum, and then starts to diverge so that the points leave the camera field of view. Even if we do not consider this constraint (we are here in simulation where an image plane of infinite size can be assumed), the camera then reaches the object plane where $Z = 0$, leading of course to a failure. From the results depicted in Fig. 4.b and 4.c, we can see that control laws C and A both fail in a local minimum. As for control

law A, it is the first time, as far as we know, that such a local minimum problem is exhibited. Finally, control law G is the only one to converge to the desired pose as soon as $0.515 < \beta < 0.569$ (see Fig. 4.d). The oscillations observed in the camera velocity and in the points coordinates allow the camera to go out from the workspace corresponding to the attractive area of the local minimum for the other control schemes.

5. CONCLUSIONS

The control laws used in image-based visual servoing have their respective drawbacks and strengths. In some cases, a control law is not able to converge while the others succeed. In other cases, all classical control laws may fail. Different behaviors may explain these failures. For example, the camera moves to infinity, the camera moves to be too near to the object, the camera reaches a local minimum or a singular configuration. In this paper, new configurations have been exhibited, for the first time as far as we know: a local minimum for all classical control schemes, especially for the control law proposed in [14]. A singularity of the control scheme proposed in [14] has also been exhibited and its effects have been emphasized through experiments obtained on a 6 dof robot. New surprising results have also been obtained for the other classical control schemes for motion combining translation along and rotation around the optical axis. Finally, a new control law based on a behavior controller has also been proposed. Setting $\beta = 0, 1$, or $1/2$ would allow to switch between the three most classical schemes but we have preferred to analyse the behavior of the control scheme for all possible values of this parameter. In all considered cases (difficult configurations subject to local minima for all classical schemes, motion along and around the optical axis), it has always been possible to determine values of this parameter that provide a satisfactory behavior of the control scheme. In fact, the suitable values of the behavior controller rely on the displacement that the camera has to realize. Future work will

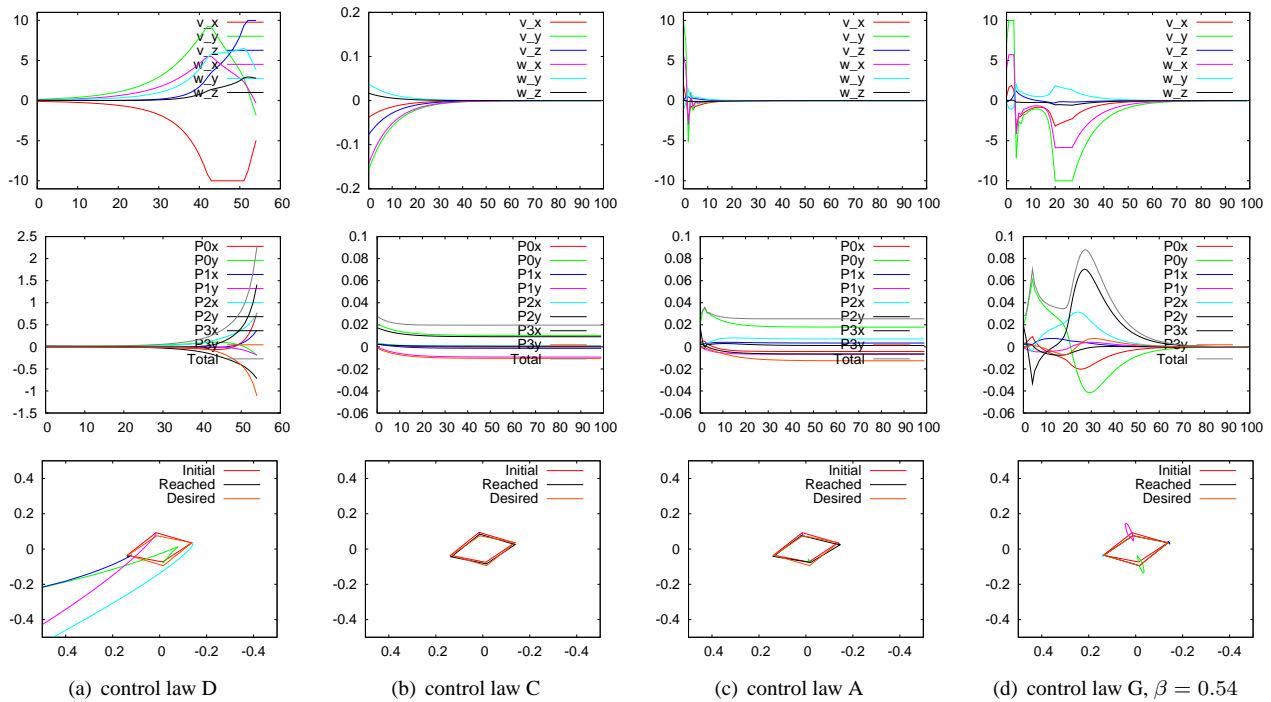


Fig. 4. Simulation results for local minima situation

thus be devoted to determining how to select automatically the value of the behavior controller to obtain a good behavior in all cases. Modifying on line the value of the behavior controller during the task execution will be also studied.

ACKNOWLEDGMENTS

The authors would like to thank Seth Hutchinson for his comments on this research and earlier draft of this paper.

REFERENCES

[1] A. H. Abdul Hafez and C.V. Jawahar. Visual servoing by optimization of a 2D/3D hybrid objective function. ICRA'07, pp. 1691-1696, Apr. 2007.

[2] E. Cervera, A. Pobil, F. Berry and P. Martinet. Improving image-based visual servoing with three-dimensional features. Int. Journal of Robotics Research, 22:821-839, Oct. 2003.

[3] F. Chaumette. Potential problems of stability and convergence in image-based and position-based visual servoing. The Conference of Vision and Control. LNCIS 237, pp 66-78, Springer Verlag, 1998.

[4] F. Chaumette. Image moments: a general and useful set of features for visual servoing. IEEE Trans. on Robotics and Automation, 20(4):713-723, Aug. 2004.

[5] F. Chaumette and S. Hutchinson. Visual servo control Part I: basic approaches. IEEE Robotics and Automation Magazine, 13(4):82-90, Dec. 2006.

[6] P. Corke and S. Hutchinson. A new partitioned approach to image-based visual servo control. IEEE Trans. on Robotics and Automation, 17(4):507-515, Aug. 2001.

[7] L. Deng, F. Janabi-Sharifi and W. Wilson. Hybrid strategies for image constraints avoidance in visual servoing. IROS02, Lausanne, pp 348-353, Oct. 2002.

[8] B. Espiau, F. Chaumette and P. Rives. A new approach to visual servoing in robotics. IEEE Trans. on Robotics and Automation, 8(3):313-326, June 1992.

[9] N. Gans, S. Hutchinson and P. Corke. Performance tests for visual servo control systems, with application to partitioned approaches to visual servo control. Int. Journal of Robotics Research, 22:955-981, Oct. 2003.

[10] N. Gans and S. Hutchinson. Stable visual servoing through hybrid switched-systems control. IEEE Trans. on Robotics, 23(3):530-540, June 2007.

[11] S. Hutchinson, G. Hager and P. Corke. A tutorial on visual servo control. IEEE Trans. on Robotics and Automation, 12(5):651-670, Oct. 1996.

[12] F. Janabi-Sharifi and W. Wilson. Automatic selection of image features for visual servoing. IEEE Trans. on Robotics and Automation 13(6):890-903, Dec. 1997.

[13] E. Malis, F. Chaumette and S. Boudet. 2 1/2 D visual servoing. IEEE Trans. on Robotics and Automation, 15(2):238-250, Apr. 1999.

[14] E. Malis. Improving vision-based control using efficient second-order minimization techniques. ICRA'04, pp 1843-1848, New Orleans, Apr. 2004.

[15] E. Marchand, F. Spindler, F. Chaumette. ViSP for visual servoing: a generic software platform with a wide class of robot control skills. IEEE Robotics and Automation Magazine, 12(4):40-52, Dec. 2005.

[16] P. Martinet, J. Gallice and D. Khadraoui. Vision based control law using 3d visual features. Second World Automation Congress, Vol. 3, pp. 497-502, Montpellier, France, May 1996.

[17] O. Tahri, Y. Mezouar. On the efficient second order minimization and image-based visual servoing ICRA'08, Pasadena, May 2008.

[18] W. Wilson, C. Hulls and G. Bell. Relative end-effector control using Cartesian position based visual servoing. IEEE Trans. on Robotics and Automation, 12(5):684-696, Oct. 1996.